

Cite this: *Sustainable Food Technol.*,  
2025, 3, 1086

# Dielectric barrier discharge cold plasma-modified pea protein nanoparticles: enhancing functional and thermal properties for food and biopolymer applications

Srutee Rout \* and Prem Prakash Srivastav

This study explored the use of dielectric barrier discharge cold plasma (DBD-CP) to produce Pea Protein Isolate Nanoparticles (PPI-NPs) at 30 kV for 2, 4, 6, and 8 min. Increasing the voltage and extending the treatment time led to larger nanoparticle sizes and more irregular morphology. Samples treated with CP showed higher absorbance in the 230–300 nm range, while fluorescence intensity decreased as the treatment time increased. CP exposure altered the FTIR spectra, particularly the amide I and II bands. The plasma-treated PPI-NPs exhibited increased surface hydrophobicity and carbonyl content and reduced free sulfhydryl (SH) groups compared to untreated samples. Additionally, the water and oil holding capacities and solubility of PPI-NPs improved with longer treatment durations. Thermal analysis revealed that CP exposure at 30 kV for 6 and 8 min increased the denaturation temperature ( $T_d$ ) to 112 °C and 114 °C, respectively. At the same time, the untreated sample had a  $T_d$  of 110 °C, indicating enhanced cross-linking of polar functional groups. These results suggest that CP treatment effectively improves the functional properties of protein nanoparticles, making them suitable for applications in food packaging and pharmaceuticals.

Received 30th March 2025  
Accepted 28th April 2025

DOI: 10.1039/d5fb00123d

rsc.li/susfoodtech

## Sustainability spotlight

The synergistic modification of pea protein isolate (PPI) using Dielectric Barrier Discharge Cold Plasma (DBD-CP) technology offers a sustainable and eco-friendly approach to developing protein nanoparticles with enhanced thermal, physicochemical, and functional properties. This innovative method leverages non-thermal plasma to introduce reactive oxygen and nitrogen species (RONS), facilitating the formation of novel functional groups while minimizing the need for harsh chemicals or solvents. The resultant nanoparticles exhibit improved solubility, emulsifying capacity, and thermal stability, making them suitable for diverse applications in the food and biopolymer industries. Moreover, DBD-CP treatment aligns with sustainable processing goals by reducing energy consumption, minimizing waste, and enhancing resource efficiency. Incorporating modified PPI-NPs into food matrices and biodegradable polymer systems contributes to improved product performance and supports the development of sustainable, high-value products, thereby advancing the circular bioeconomy.

## 1. Introduction

Protein nanoparticles have gained considerable attention in the food industry due to their nanoscale size and high surface-area-to-volume ratio. According to Rasool *et al.*, nanoparticles are characterized by having at least one dimension measuring less than 1000 nm, although this threshold can differ based on the material type.<sup>1</sup> Their minute size enhances dispersibility, gravitational separation, stability, aggregation, and structural changes during food processing. In recent years, biopolymer-based nanoparticles have been widely explored in functional foods and pharmaceuticals as effective encapsulation and delivery systems.<sup>2</sup> Their biocompatibility, edibility, and

Generally Recognized as Safe (GRAS) status make them ideal for incorporation into food systems. These nanoparticles can significantly enhance the solubility of hydrophobic bioactive compounds prone to oxidation, improve stability during storage or under adverse conditions, regulate controlled release in the gastrointestinal tract, and enhance bioaccessibility and bioavailability. Proteins are highly suitable for nanoparticle formulation owing to their amphiphilic characteristics, which enable them to engage efficiently with both solvents and dispersed phases.<sup>3</sup> Traditionally, proteins derived from animal sources, such as casein, gelatin, whey protein, and  $\beta$ -lactoglobulin, have been employed in nanoparticle synthesis. However, plant-based proteins from sources such as soybeans, pulses, legumes, and cereals offer a sustainable and abundant alternative.<sup>4</sup> These plant-derived proteins, categorized as GRAS, provide notable advantages in food applications. Food proteins exhibit exceptional functional properties among all GRAS

Department of Agricultural and Food Engineering, Indian Institute of Technology Kharagpur, Kharagpur, West Bengal 721302, India. E-mail: sruteerout1997@gmail.com; Tel: +91-6372757665



biopolymers, including emulsification capacity, flexibility, and antioxidant activity, making them suitable for nanoparticle-based applications.<sup>5</sup> In recent years, nanoparticles derived from proteins such as casein, egg white protein, alpha-lactalbumin, pea protein, zein, and soy protein have been developed to enhance the solubility, bioavailability, and stability of nutraceuticals. These protein-based NPs can be synthesized using various techniques, including desolvation, enzyme- or calcium-induced cross-linking, self-assembly, heat-induced aggregation, and cold-gelation.<sup>6</sup>

Pea proteins primarily consist of globulins and smaller fractions of albumins and glutelins.<sup>7,8</sup> The major globulin component is legumin, a hexameric 11S globulin with a molecular mass ranging from 350 to 400 kDa, rich in  $\beta$ -sheet structures and stabilized by disulfide bridges. A minor glycoprotein fraction known as vicilin, a trimeric 7S globulin with an approximate molecular mass of 150 kDa, is also present. Pea proteins exhibit high solubility at pH values far from their isoelectric point, though their solubility drops to around 30% near pH 5.<sup>9</sup> Pea proteins demonstrate strong potential in gelation, foaming, film formation, and emulsion stabilization, making them highly versatile in food systems.<sup>10</sup> Pea protein is a significant contender in the global plant-based protein market. However, despite its many advantages, PPI-NPs exhibit limitations such as low water solubility, reduced foaming and emulsifying properties, and limited digestibility due to their high protein content.<sup>11</sup> Various modification techniques have been explored to enhance its functionality for broader use in food applications. In particular, developing nano- and microparticles from pea protein has gained attention as a promising strategy to improve its performance in diverse formulations. For instance, Jhan *et al.* successfully used legumin to produce nanoparticles with diameters ranging from 200 to 700 nm using glutaraldehyde as a crosslinking agent, while coacervation using whole pea proteins yielded microparticles with sizes ranging from 10  $\mu$ m to several hundred  $\mu$ m.<sup>12</sup>

DBD-CP is an innovative and non-thermal technology recognized for its cost-effectiveness, chemical-free nature, and high energy efficiency, achieved through gas ionization.<sup>13–15</sup> Recently, DBD-CP has shown significant ability to modify biopolymers. Plasma consists of a complex mixture of excited and non-excited gas molecules, radicals, ions, and electromagnetic radiation.<sup>16–18</sup> These reactive species can induce physical and chemical modifications in polymers at micro- and nano-scales without altering their bulk properties. To date, DBD-CP has been extensively applied in the surface modification of biopolymers, particularly proteins. Research has shown that DBD-CP can alter protein surfaces and structures by modifying functional groups such as free sulfhydryl, carbonyl, sulphhydryl, and carboxyl groups.<sup>19</sup> Studies have demonstrated that CP technology is capable of fabricating synthetic nanostructures with hydrophilic and superhydrophobic surfaces, with the latter offering diverse applications in nanotechnology and interface science. As a result, there is growing interest in harnessing plasma technology for the fabrication of biopolymer nanoparticles. Previous research had confirmed that CP is an effective method for modifying pea protein aggregates that improved

physicochemical and functional properties.<sup>11</sup> Therefore, this study explores the potential of DBD-CP to fabricate PPI-NPs at 30 kV with treatment durations of 2, 4, 6, and 8 min. Additionally, the research investigates the mechanisms of PPI-NP formation through CP technology by analyzing the chemical and structural modifications, morphology, interactive forces, and particle size distribution, all of which stabilize the nanoparticle structure.

## 2. Materials and methods

### 2.1. Materials

PPI was purchased from Profoods Nutrition. All other materials used in this study were of analytical grade and procured from Sigma, HiMedia, and Merck, India.

### 2.2. DBD-CP treatment of PPI

CP treatments were conducted using a voltage generator and a plasma treatment chamber. The chamber was equipped with parallel copper electrodes, each 5 mm thick and positioned 15 mm apart. These electrodes were covered with thick quartz dielectric barrier (DB) plates. A 230 V, 50 Hz power supply was used to energize the primary winding of a high-voltage step-up transformer. The CP setup, was assembled with two metal electrodes positioned around a Petri plate containing 20 g of solid PPI powder placed on the sample stage. The CP treatment was applied at an output voltage of 30 kV for varying durations of 2–8 min. The parameters were precisely regulated through a control panel integrated with the step-up transformer. Following treatment, the processed PPI powder was stored in airtight polybags for further analysis.

### 2.3. Preparation of PPI-NPs

Protein nanoparticles were produced using a modified version of the method outlined by Liang *et al.*<sup>20</sup> Both native and CP-treated PPI samples were combined with 400 mL of distilled water and heated to 95 °C with continuous stirring for 30 min. Ethanol was then gradually added to the protein solution while maintaining constant agitation. After cooling the suspension to room temperature, an additional amount of ethanol was introduced dropwise, followed by continuous stirring for another 20 min. The resulting nanoparticle suspension was centrifuged at 4000 $\times$ g for 10 min. The collected sediment was rinsed twice with ethanol to remove any remaining moisture and subsequently dried at 45 °C for 24 h, reducing the moisture content to around 10% on a wet basis.

### 2.4. Surface characterization of PPI-NPs

A 2% (w/v) protein suspension was prepared in 10 mM phosphate-buffered saline (PBS) with an initial pH of 6.8, which was subsequently adjusted to pH 7.0 using either an acid or a base according to the method of Liu *et al.*<sup>21</sup> The hydrodynamic diameter of the particles at pH 7.0 was determined through dynamic light scattering (DLS). Prior to analysis, each sample was diluted 100-fold using ultrapure water. The measurements



were analyzed using Malvern Zetasizer software, and all experiments were conducted in triplicate.

### 2.5. Chemical characteristics of PPI-NPs

The chemical properties resulting from plasma treatment, such as the total content of protein carbonyl groups and SH groups, and surface hydrophobicity, were analyzed following the methodology described in our previous study.<sup>11</sup> The reported data are represented as the average values obtained from triplicates.

### 2.6. Circular dichroism (CD) of PPI-NPs

The alterations in the secondary structure of PPI-NPs were analyzed using Far-UV CD spectra by a modified method of Marques *et al.*<sup>22</sup> The protein concentration was maintained at 0.2 mg mL<sup>-1</sup>, and measurements were conducted at 25 °C with an optical path length, covering the wavelength range of 180–270 nm. The speed of scanning was set at 50 nm min<sup>-1</sup>, with a spectral resolution of 0.1 nm, response time of 0.1 s, and bandwidth of 1 nm.

### 2.7. Protein solubility of PPI-NPs

The solubility of both native and treated PPI-NPs was assessed using the Kjeldahl method following the procedure outlined in Wu *et al.*<sup>23</sup> All samples were stirred vigorously with a high-speed magnetic stirrer and then centrifuged at 9000×*g* for 20 min. The protein content of the supernatant was analyzed using the Kjeldahl method, and protein solubility was calculated using eqn (1).

$$\text{Protein solubility(\%)} = \frac{\text{Supernatant protein}}{\text{Total protein in powder}} \times 100 \quad (1)$$

### 2.8. Free amino groups

The orthophthalaldehyde (OPA) colorimetric assay was utilized to determine the concentration of available amino groups in PPI-NPs, by the method outlined by Chen *et al.*<sup>24</sup> The process involved dissolving the OPA reagent in 2 mL of 95% ethanol, followed by the addition of 50 mL of 100 mM sodium tetraborate buffer, 5 mL of SDS solution, and 200 μL of β-mercaptoethanol. The mixture was then diluted to a final volume of 100 mL using distilled water. To initiate the assay, 1.5 mL of an OPA solution (1 mg mL<sup>-1</sup>) was introduced. The solution was vortexed for 3 min in a dark environment at room temperature, followed by the measurement of absorbance at 340 nm using a UV/vis spectrophotometer.

### 2.9. Differential scanning calorimetry (DSC)

A PerkinElmer Pyris Diamond DSC was utilized to investigate the thermal properties of PPI-NPs following CP treatment by the method of Angourani *et al.*<sup>25</sup> Approximately, 2 mg of each sample was placed in aluminum liquid pans (Dupont) with 10 mL of 0.1 M phosphate buffer (pH 7.0). The pans were then tightly sealed and subjected to a controlled heating process, ranging from 20 °C to 120 °C at a rate of 5 °C min<sup>-1</sup>. The

thermograms obtained were analyzed to determine the key thermal parameter  $T_d$  using Universal Analysis 2000 software. Each experiment was conducted in triplicate, and prior to testing, the sealed pans containing the samples were conditioned at 20 °C for a minimum of 6 h.

### 2.10. TGA

Thermal analysis (TG/DTG/DTA) was conducted using a PerkinElmer Pyris Diamond TG-DTA system under a nitrogen atmosphere according to the method of Angourani *et al.*<sup>25</sup> Approximately 5 mg of the powdered sample was accurately weighed and placed into a ceramic crucible. The sample was then heated from room temperature to 800 °C at a constant rate of 10 °C min<sup>-1</sup>, with a nitrogen gas flow maintained at 60 mL min<sup>-1</sup>. Differential thermal analysis (DTA) curves were generated by taking the first derivative of the TGA data. The temperature corresponding to the maximum rate of thermal decomposition was identified from the DTA curves.

### 2.11. Morphology of PPI-NPs

The surface morphology of CP-treated and control protein isolates was analyzed using a MERLIN FESEM (Carl Zeiss, Oberkochen, Germany). The samples were mounted on cylindrical specimen holders and coated with a thin layer of gold before imaging. The examination was conducted at 20 kV with magnifications ranging between 1000 and 3000.

### 2.12. Statistical analysis

All experiments were carried out in triplicate. Statistical analysis was conducted using IBM SPSS Statistics, with ANOVA applied at a 95% confidence level ( $p < 0.05$ ). Tukey's HSD test was employed to determine significant differences between the means.

## 3. Results and discussion

### 3.1. UV absorption and fluorescence intensity analysis

The UV-vis spectrum of proteins is influenced by the absorbance peaks of aromatic amino acids, including “phenylalanine (250–265 nm)”, “tryptophan–tyrosine (265–280 nm)”, and “tryptophan (285–300 nm)”. Fig. 1a illustrates the UV-vis spectra of both untreated and CP-treated PPI-NPs. Compared to the control, the treated samples exhibited higher absorbance in the 230–300 nm range. The CP-treated proteins demonstrated a significant increase in absorption intensity, primarily attributed to alterations in hydrophobic groups and the exposure of aromatic residues. This enhanced absorbance suggests that protein denaturation caused by CP treatment exposes more chromophores on the protein surface, thereby increasing UV-vis absorption. The results are in accordance with previous studies reported by Nasiru *et al.*<sup>26</sup> Notably, at 30 kV for 8 min, the absorbance intensity was lower than those at 4 and 6 min, likely due to a combination of protein conformational changes and oxidative degradation of tryptophan residues. This process can expose or bury tyrosine and tryptophan residues, leading to variations in absorption intensity. These findings highlight the



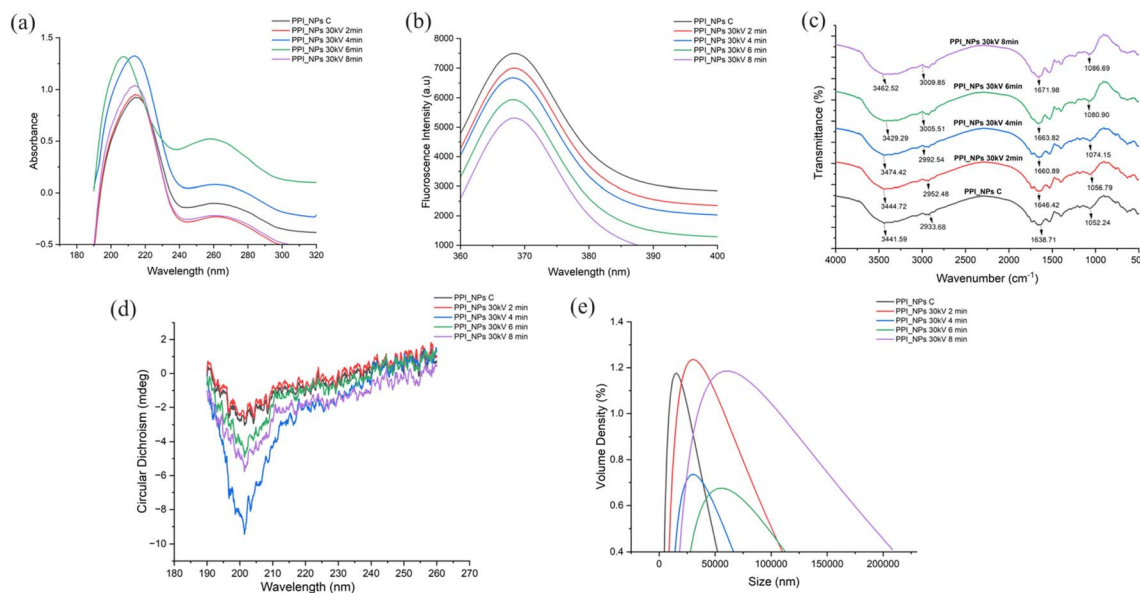


Fig. 1 Dielectric bath discharge cold plasma treatment of PPI-NPs as tested by (a) UV absorption spectra, (b) fluorescence absorption spectra and secondary structures reported by (c) FTIR analysis, (d) circular dichroism spectra, and (e) particle size.

capability of CP treatment to modify the physicochemical characteristics of pea proteins by triggering structural changes at the molecular level.<sup>27,28</sup> The differences in tertiary structure of proteins can be assessed using the intrinsic fluorescence of tryptophan, which is highly susceptible to the polarity of its surrounding microenvironment.<sup>29</sup> Due to this sensitivity, tryptophan residues are commonly used to monitor structural changes in proteins. The fluorescence spectrum (Fig. 1b) was generated by exciting hydrophobic amino acid residues to analyze alterations in the tertiary structure of proteins.<sup>30</sup> As shown in Fig. 1b, an increase in CP treatment time led to a gradual decline in the fluorescence intensity of PPI-NPs, indicating structural modifications. This reduction suggests that tryptophan residues may have migrated from a hydrophobic environment to a more hydrophilic one. The decline in fluorescence intensity could also be attributed to reactive oxygen species (ROS) generated during plasma exposure, which are known to act as early markers of free radical-induced protein oxidation, ultimately leading to decreased fluorescence.<sup>31</sup> Since most hydrophobic aromatic amino acids in PPI are typically found within the hydrophobic core, any conformational change caused by CP treatment would result in reduced fluorescence intensity.<sup>32</sup> Similar structural alterations have been reported for whey, soy, tropomyosin and peanut proteins following CP treatment, where the fluorescence intensity decreased due to the disruption of hydrogen bonding under alkaline conditions. The combined results from fluorescence and FTIR analysis indicate that CP treatment induces structural changes primarily at the tertiary level.<sup>33–35</sup> A comparable trend was observed by Li *et al.*, who reported a gradual decrease in tryptophan fluorescence intensity at 355 nm in PPI following CP treatment for 1 to 10 min.<sup>36</sup> This reduction is likely due to tryptophan oxidation, which results in the formation of carbonyl groups, along with structural modifications occurring

during CP exposure. These observations are consistent with the findings of CP-treated grass pea protein isolates where the fluorescence intensity decreased.<sup>32</sup>

### 3.2. FTIR analysis

The changes in the chemical compounds of PPI-NPs in native and CP-treated samples over time were analyzed using FTIR spectroscopy, as illustrated in Fig. 1c. The amide A and B regions “3100–3600  $\text{cm}^{-1}$ ” exhibited broad absorption peaks, attributed to the “O–H (3200–3550  $\text{cm}^{-1}$ )” and “N–H (3300–3400  $\text{cm}^{-1}$ )” stretching vibrations of PPI. As reported by Pasieczna-Patkowska *et al.*, the amide I band “(1600–1700  $\text{cm}^{-1}$ )” primarily arises from C=O stretching vibrations (70–85%) and the hydrogen bonding patterns associated with the secondary structure.<sup>37</sup> Following CP treatment, there was a slight increase in the N–H bond indicating a partial breakdown of peptide bonds in PPI. The peak intensity of the amide I (1638  $\text{cm}^{-1}$ ) and amide II bands was reduced in CP-treated PPI-NPs, suggesting peptide chain cleavage due to interactions with reactive plasma species.

In addition, the CP-treated samples exhibited decreased intensity at 1450 and 1392  $\text{cm}^{-1}$ , reflecting scissions in amino acid residues with methyl side chains ( $-\text{CH}_3$  and  $-\text{CH}_2$ ), respectively.<sup>38</sup> Oxidative modifications induced by hydroxyl radicals also contributed to structural changes, particularly affecting aromatic amino acids such as tyrosine, phenylalanine, and tryptophan. Similar changes were observed in studies examining the effects of CP on mung bean protein.<sup>39</sup> The predominant peak observed in mung bean seeds was at 1633.37  $\text{cm}^{-1}$ , corresponding to the presence of proteins. Another peak, identified at 3322.16  $\text{cm}^{-1}$ , was attributed to the stretching vibrations of hydroxyl and NH groups associated with alcohols. Jahromi *et al.* observed that sodium caseinate powders treated for varying durations showed no notable changes in the amide I and amide



II regions.<sup>40</sup> However, a minor shift was recorded in the amide III band associated with N–H in-plane bending and C–N stretching moving from 1238 cm<sup>-1</sup> in the untreated sample to 1234, 1234, and 1230 cm<sup>-1</sup> after 2.5, 5, and 10 min of treatment, respectively. Additionally, the signal at 976 cm<sup>-1</sup> gradually weakened with prolonged treatment, suggesting mild oxidation and structural degradation in the 10 min sample. Similarly, in both native and CP-treated egg white protein (EWP), the amide A peak, typically resulting from N–H or O–H stretching, remained consistent, while the amide B peak linked to C–H bending vibrations shifted slightly from 2960 cm<sup>-1</sup> in the untreated sample to a range of 2962–2964 cm<sup>-1</sup> after plasma exposure, likely due to depolymerization effects. Both treated and native EWP samples exhibited a band at 1633.41 cm<sup>-1</sup>, attributed to C–O and C–N stretching vibrations.<sup>41</sup>

### 3.3. CD spectroscopy

The structural effects of CP treatment on PPI-NPs were assessed.<sup>42</sup> As depicted in Fig. 1d, prolonged CP exposure led to a gradual reduction in “ $\alpha$ -helix” content, while the proportions of “ $\beta$ -strands” and “ $\beta$ -turns” fluctuated in both protein isolates. Notably, PPI-NPs treated at 30 kV for 4 min showed a significant alteration in the intensity of the negative peak at approximately 208 and 222 nm when compared to the control. This change could be due to the effect of insoluble particles on light scattering, which altered the absorption of plane-polarized light. While a minor shift in the intensity of the negative peak was noticeable after treatment at 30 kV for 4 minutes, negligible differences were observed in samples exposed for 2 and 6 min. According to reported studies, plasma treatment significantly affects the  $\alpha$ -helical and  $\beta$ -sheet regions of various proteins, including whey proteins,<sup>43</sup> peanuts,<sup>44</sup> and oats.<sup>45</sup> Similarly, Rout & Srivastav reported that direct plasma treatment reduced the  $\alpha$ -helix and  $\beta$ -turn content in lactate dehydrogenase while augmenting the proportion of  $\beta$ -strands.<sup>41</sup> These findings highlight the potential of CP treatment to induce structural modifications in plant and animal proteins, affecting their functional and physicochemical properties.

The spectra exhibiting a negative peak near 208 nm and a positive peak around 195 nm are characteristic of  $\beta$ -sheet and  $\alpha$ -helical structural conformations.<sup>46</sup> In this study, two prominent negative peaks (~200 nm) and positive peaks (~187 nm) were identified, indicating the presence of  $\alpha$ -helical and  $\beta$ -sheet structures. A slight shift (~8 nm) in the spectra could be attributed to the presence of non-protein components, as CD spectroscopy is highly sensitive to even minor structural variations.<sup>47</sup> As a result of this sensitivity, the analyzed oat protein samples exhibited a comparatively higher proportion of unordered coil structures. The secondary structure of oat protein is predominantly composed of  $\alpha$ -helices,  $\beta$ -sheets, and turns. Additionally, a subtle shoulder peak was observed within the 212–225 nm range, which is indicative of  $\beta$ -sheet regions. This finding aligns with previously reported CD spectral analyses of oat protein, confirming the structural characteristics of oat protein and its diverse conformational elements.<sup>45</sup>

### 3.4. Particle size distribution

Fig. 1e shows the size distribution of PPI-NPs. The pea protein dispersions displayed a monomodal particle distribution. Notably, CP-treated protein nanoparticles exhibited a larger particle size than the control.<sup>7</sup> For the plasma-treated samples, the peak shifted to the right at 30 kV, indicating an increase in particle size. This shift may be attributed to aggregation caused by plasma, where energetic plasma species influence the charge distribution on and around protein particles, reducing electrostatic repulsion and promoting particle aggregation. Additionally, the exposure of protein molecules to high-energy plasma species may lead to protein unfolding, exposing hydrophobic regions to the surface, subsequently increasing surface hydrophobicity.<sup>21</sup> This enhanced hydrophobicity further facilitates the flocculation of protein particles, resulting in larger particle sizes. These findings align with previous research, which reported similar aggregation effects induced by CP treatment in oat milk,<sup>48</sup> soybean protein isolates,<sup>49</sup> and pea protein isolates.<sup>11</sup> Prolonged plasma treatment can promote the formation of supramolecular structures with a larger hydrodynamic radius, potentially driven by intra- or intermolecular crosslinking, electrostatic forces, or hydrophobic interactions, as demonstrated by Hekmat *et al.*<sup>50</sup>

### 3.5. Thermal characteristics of PPI-NPs

DSC is a valuable technique for analyzing the thermodynamic stability of proteins. The DSC curves of different samples reveal variations in the denaturation temperature, which correlates with the energy required to disrupt protein structures.<sup>51</sup> A  $T_d$  signifies greater structural stability, whereas a lower glass transition temperature suggests reduced molecular weight conversion, potentially enhancing protein digestibility. This analytical approach provides insights into structural transitions, including protein denaturation and starch gelatinization, during food processing.<sup>52</sup> The DSC thermograms of both native and CP-treated PPI-NPs, as depicted in Fig. 2a, display multiple endothermic peaks, indicating thermal transitions associated with different protein aggregates exhibiting distinct denaturation temperatures. A broad endothermic peak, observed between 40 and 150 °C, corresponds to protein denaturation.<sup>53</sup> The untreated sample exhibited a denaturation temperature of 110 °C, whereas CP treatment at 30 kV for 6 and 8 min elevated  $T_d$  to 112 °C and 114 °C, respectively. This increase suggests enhanced cross-linking of polar functional groups and partial denaturation within the PPI structure, demonstrating a direct correlation between CP treatment duration and thermal stability. These findings are consistent with Perinban *et al.*, who reported  $T_d$  values ranging from 102 to 109 °C for CP-treated whey protein isolates.<sup>54</sup> A similar trend was reported for zein protein, where the denaturation temperature decreased from 77.10 °C (native) to 65.90 °C following 125 V plasma treatment, suggesting the disruption of intermolecular interactions such as triple and double bonds, thereby reducing denaturation energy requirements.<sup>55</sup> The DSC results further support FTIR findings, which indicate modifications in the protein bonding structure. Another study observed that the  $T_d$  of untreated PPI films increased from 61.16 °C to 72.56 °C after 30 s of CP exposure.<sup>56</sup> Similarly, Mehr &





Fig. 2 (a) DSC, (b) TGA, (c) DTA, and (d) DTG thermograms of native and treated PPI-NPs.

Koocheki reported a significant increase in  $T_d$  for grass pea protein isolates after CP treatment, attributing this change to protein aggregation.<sup>32</sup> The overall rise in  $T_d$  following CP treatment enhances the thermal stability of PPI, making it a promising constituent for applications in the food industry, particularly in product formulation and packaging.

TGA and DTA are used to monitor changes in the weight and rate of weight loss of a material over time or at varying temperatures.<sup>57</sup> These changes occur due to processes such as vaporization, decomposition, and oxidation. TGA is primarily employed to assess the composition of materials and predict their thermal stability at elevated temperature. The TGA results (Fig. 2b) reveal the percentage of weight loss relative to the initial sample weight, while the DTA curve (Fig. 2c) provides information on the rate of decomposition with respect to temperature. Both plasma-treated and untreated PPI-NPs were subjected to TGA and DTA analysis. In this study, all samples exhibited a three-stage weight loss pattern. The initial weight reduction occurred due to the loss of moisture and volatile compounds. The second stage, occurring between approximately 120 °C and 330 °C, was characterized by a rapid decline in weight indicating thermal degradation. The final stage, between 390 °C and 540 °C, involved carbonization, during which most functional groups were eliminated.<sup>58</sup> This stage likely corresponds to the breakdown of high-molecular-weight bonds as the polymer undergoes structural disintegration within this temperature range.

CP treatment influenced the thermal decomposition characteristics of PPI-NPs by altering the composition of lower molecular weight proteins.<sup>59</sup> These modifications likely resulted from protein aggregation or breakdown due to extended CP

exposure and increased discharge intensity. At 30 kV for 2 and 8 min, CP treatment did not significantly affect the weight loss of PPI-NPs. However, at 30 kV for 4 and 6 min, the thermal stability improved across all phases, leading to a noticeable reduction in weight loss. This enhancement is attributed to CP-induced cross-linking between protein molecules, which strengthened intermolecular interactions and created a more stable protein network. The reactive species generated during CP exposure contributed to the formation of disulfide bonds and covalent linkages, reinforcing the protein structure and making it more resistant to thermal degradation.

Despite this structural enhancement, degradation temperatures for CP-treated PPI-NPs at 28 kV (6 and 8 min) decreased from 336 °C to 321.5 °C and 315.6 °C, respectively, compared to untreated samples. This decline suggests protein unfolding, partial dehydration, and polypeptide chain rearrangement induced by CP exposure.<sup>60</sup> Analysis of the derivative thermogravimetric (DTG) curves (Fig. 2d) revealed that maximum degradation in untreated samples occurred at approximately 310 °C, whereas in CP-treated samples, it occurred around 295 °C. This shift indicates that CP-treated proteins degraded at lower temperatures than their untreated counterparts, demonstrating an improvement in thermal stability. Research by Kumar *et al.* also highlighted enhanced thermal stability and water-holding capacity in PPI-alginate (PPI-AG) complexes after CP treatment.<sup>61</sup> Similarly, Santosh *et al.* reported improved thermal stability in PPI films due to increased  $\beta$ -sheet structures following CP exposure.<sup>56</sup> Additionally, a study by Rachtanapun *et al.* found that incorporating 10% polyethylene (PE) into rice starch/carboxymethyl chitosan films significantly enhanced their thermal resistance.<sup>62</sup>



### 3.6. Free amino groups

The interaction of OPA with protein particles was utilized to analyze conformational changes and determine the content of terminal  $\alpha$ -NH<sub>2</sub> groups of peptides and  $\epsilon$ -NH<sub>2</sub> groups of lysine on the surface of PPI-NPs after CP treatment.<sup>63</sup> Significant alterations in the free amino content (FAC) of PPI-NPs were observed as shown in Fig. 3a, with variations notably influenced by the duration of CP treatment ( $P < 0.05$ ). FAC increased from 12.23% in untreated PPI-NPs to 14.54% and 12.78% after CP exposure at 30 kV for 2 min and 8 min, respectively. This increase suggests that CP treatment induced surface etching, which disintegrated primary PPI-NP aggregates and led to the formation of extended protein conformations, consistent with FTIR findings. Mehr & Koocheki<sup>32</sup> highlighted that the initial stages of CP treatment could oxidize surface-exposed methionine and cysteine residues, triggering extensive conformational changes that expose reactive  $\epsilon$ -NH<sub>2</sub> lysine groups on the particle surface. However, the oxidation rate depends on factors such as peptide bond flexibility, ROS concentration, protein conformation, and amino acid surface accessibility.<sup>64</sup> Open bonds accelerate chemical etching due to the ROS generated during plasma treatment.<sup>32</sup> As a result, the high etching efficiency observed at 30 kV enhances the exposure of free amino groups during the initial phase of plasma treatment. This increased accessibility, combined with a higher density of reactive plasma species, promotes the oxidation of a significant proportion of free amino groups, ultimately reducing OPA reactivity in PPI-NPs treated for 8 min. In contrast, reduced etching efficiency and a lower concentration of reactive species during extended plasma exposure slow down the oxidation process of free amino groups, thereby requiring prolonged treatment times to achieve a further decline in OPA reactivity in CP-treated PPI-NPs.

### 3.7. Water/oil holding capacity (WHC/OHC) and water absorption capacity (WAC)

WHC and OHC refer to the ability of food systems to retain water and oil, respectively, which are critical properties influencing the texture of foods such as baked dough, minced meat, and dairy products.<sup>65</sup> Plasma treatment significantly enhanced the water

and oil absorption capacities of PPI-NPs at 30 kV for 6 min, increasing the WHC and OHC from  $29.54 \pm 1.32$  and  $26.69 \pm 1.18$  to  $31.80 \pm 1.29$  and  $34.17 \pm 1.42$ , respectively (Table 1). This improvement is likely due to the greater exposure of soluble proteins and polar amino acids along the protein chain. The ionization of these polar amino acids within the reactive plasma environment may have influenced the WHC, facilitating better water retention. CP treatment promotes protein chain unfolding, the incorporation of hydrophilic groups on the surface, and the fragmentation of extended amyloid chains, all of which enhance water absorption.<sup>11</sup> Additionally, the reactive species produced during CP treatment can induce surface oxidation of the granules, resulting in an elevated surface charge and promoting the attachment of polar functional groups. This ultimately boosts water absorption capacity. Similar trends were observed when exposing flour fractions to CP treatment for up to 10 min, which resulted in a gradual increase in water binding capacity (WBC) by 113% in Protein Rich Peanut Flour (PPF) and 106% in Pea Testa Flour (PTF).<sup>15</sup> The observed enhancement in the WHC is consistent with the improved hydrophilicity in CP-treated pea protein isolates. Table 1 illustrates the WAC of control and CP-treated PPI-NPs. Compared to the control sample, a 1.42-fold increase in WAC was observed after 6 min of CP treatment at 30 kV, but a decline occurred with an 8 min treatment. This reduction is likely due to interference caused by the ions and reactive species generated during prolonged plasma exposure, which can hinder further improvement in the WAC. The corresponding rise in the WAC was also evident as the OHC, WHC, and solubility increased due to protein unfolding and surface etching induced by CP treatment.

### 3.8. Protein solubility

Solubility is a key functional attribute influencing the functional properties of proteins. CP treatment promotes solubility by generating reactive ions, such as -OH and -NH, which expose active protein sites, enhancing their interaction with water molecules.<sup>66</sup> As indicated in Table 1, the solubility of PPI-NPs improved significantly after CP treatment at 30 kV for longer durations compared to the untreated sample. This is likely due

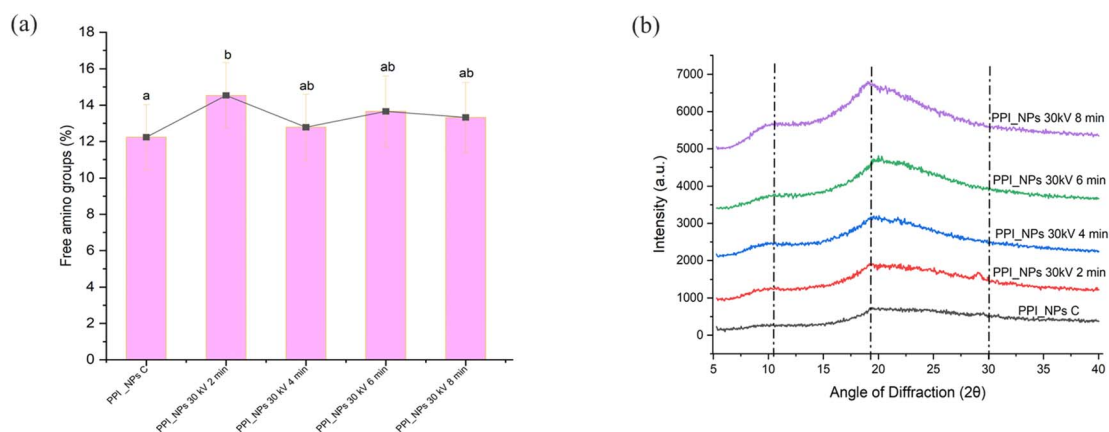


Fig. 3 (a) Free amino groups and (b) XRD spectra of native and treated PPI-NPs.



to structural modifications induced by plasma that facilitated water interaction.

The enhancement in solubility may be attributed to the oxidation effects caused by ROS and radicals generated during CP treatment. These species can induce oxidation, fragmentation, or polymerization of protein surfaces, leading to improved solubility. Zhang *et al.* reported a 282% increase in the solubility of Soy Protein Isolate (SPI) dispersions after subjecting them to cold plasma treatment at 120 Hz for 3 min.<sup>67</sup> Similarly, Ji *et al.* observed a notable enhancement in the solubility of peanut protein isolate after subjecting it to CP treatment for 20 min at 100 W.<sup>35</sup> These findings collectively highlight that CP treatment enhances the solubility of plant proteins by modifying their structural and surface characteristics.

### 3.9. Carbonyl groups and free sulphhydryl groups

Changes in carbonyl content serve as critical indicators for evaluating structural modifications and the degree of protein oxidation. The formation of carbonyl groups generally results from the cleavage of peptide bonds or modifications in the side chains of amino acids, especially those containing NH- or NH<sub>2</sub> groups. As shown in Table 1, the carbonyl content of PPI-NPs increased significantly with prolonged CP treatment ( $P < 0.05$ ), rising from  $80.68 \pm 4.34$  nmol mg<sup>-1</sup> to  $89.22$  nmol mg<sup>-1</sup> after 6 min of exposure. The observed increase is primarily due to the RONS, including hydroxyl radicals (<sup>•</sup>OH) and ozone, produced during CP treatment. These reactive species trigger the oxidation of amino acid side chains, resulting in structural alterations in amino acid residues and peptide chains, ultimately producing extra carbonyl groups and associated derivatives. Ommat Mohammadi *et al.* reported mild oxidation of whey protein isolate (WPI) following CP treatment, with oxidation levels increasing proportionally with treatment time.<sup>34</sup> Table 1 further highlights that the untreated samples exhibited the highest free sulphhydryl (-SH) group content. However, with increasing treatment time, the free sulphhydryl content in PPI-NPs decreased from  $5.08 \pm 0.37$  nmol mg<sup>-1</sup> to  $3.15 \pm 0.11$  nmol mg<sup>-1</sup>. This reduction is associated with structural modifications in the protein, where sulphhydryl groups from two cysteine residues, either on the same peptide chain or neighbouring chains, undergo coupling to form disulfide bonds through the formation of disulfide peroxy radicals. Moreover, ozone and <sup>•</sup>OH generated during CP exposure can oxidize amino acids, thereby reducing the available free sulphhydryl groups. This oxidative process induced by CP treatment leads to the formation of disulfide bonds and a reduction in -SH groups in PPI-NPs. Similar trends have been observed in pea protein,<sup>68</sup> zein protein,<sup>55</sup> whey protein,<sup>43</sup> and soy protein<sup>11</sup> following CP treatment, highlighting the widespread impact of CP on protein oxidation and structural modification.

### 3.10. Surface hydrophobicity

Hydrophobic interactions are essential for preserving the tertiary structure of proteins and have a profound effect on protein-protein interactions, which in turn influence the emulsifying and gelling characteristics of PPI-NPs.<sup>11</sup> As shown

Table 1 Effect of cold plasma on the different properties of PPI-NPs<sup>a,b</sup>

| Sample              | Color                      |                           | Water holding capacity (%) | Oil holding capacity (%)   | Water absorption capacity (g/g) | Solubility (%)            | Protein carbonyls (nmol g <sup>-1</sup> ) | Free sulphhydryl groups (μmol g <sup>-1</sup> ) | Surface hydrophobicity (H <sub>0</sub> ) |
|---------------------|----------------------------|---------------------------|----------------------------|----------------------------|---------------------------------|---------------------------|---|---|--|
|                     | L*                         | b*                        |                            |                            |                                 |                           |   |   |  |
| PPI-NPs C           | 83.15 ± 2.56 <sup>a</sup>  | 2.87 ± 0.17 <sup>ab</sup> | 29.54 ± 1.32 <sup>a</sup>  | 26.69 ± 1.18 <sup>a</sup>  | 13.63 ± 0.75 <sup>a</sup>       | 09.63 ± 0.48 <sup>a</sup> | 80.68 ± 4.34 <sup>bc</sup>                | 5.08 ± 0.37 <sup>c</sup>                        | 1225.95 ± 62.76 <sup>a</sup>             |
| PPI-NPs 30 kV 2 min | 83.25 ± 2.72 <sup>a</sup>  | 2.56 ± 0.15 <sup>a</sup>  | 30.11 ± 1.41 <sup>ab</sup> | 30.83 ± 1.44 <sup>b</sup>  | 16.57 ± 1.02 <sup>b</sup>       | 10.97 ± 0.62 <sup>a</sup> | 82.87 ± 4.79 <sup>c</sup>                 | 4.89 ± 0.22 <sup>b</sup>                        | 1324.81 ± 68.98 <sup>ab</sup>            |
| PPI-NPs 30 kV 4 min | 83.30 ± 2.79 <sup>ab</sup> | 2.94 ± 0.22 <sup>ab</sup> | 30.87 ± 1.25 <sup>ab</sup> | 32.50 ± 1.36 <sup>c</sup>  | 18.18 ± 1.15 <sup>c</sup>       | 12.12 ± 0.82 <sup>b</sup> | 85.63 ± 5.18 <sup>d</sup>                 | 5.95 ± 0.71 <sup>bc</sup>                       | 1445.85 ± 72.39 <sup>b</sup>             |
| PPI-NPs 30 kV 6 min | 83.16 ± 1.77 <sup>a</sup>  | 3.12 ± 0.34 <sup>c</sup>  | 31.80 ± 1.29 <sup>b</sup>  | 34.17 ± 1.42 <sup>d</sup>  | 19.41 ± 1.24 <sup>c</sup>       | 15.28 ± 0.93 <sup>c</sup> | 78.22 ± 4.49 <sup>ab</sup>                | 4.93 ± 0.13 <sup>b</sup>                        | 1321.30 ± 70.67 <sup>ab</sup>            |
| PPI-NPs 30 kV 8 min | 83.08 ± 1.63 <sup>ab</sup> | 2.45 ± 0.16 <sup>a</sup>  | 30.56 ± 1.32 <sup>ab</sup> | 32.04 ± 1.39 <sup>bc</sup> | 18.43 ± 1.19 <sup>c</sup>       | 17.67 ± 0.89 <sup>c</sup> | 76.67 ± 4.57 <sup>a</sup>                 | 3.15 ± 0.11 <sup>a</sup>                        | 1244.72 ± 63.78 <sup>a</sup>             |

<sup>a</sup> Data are expressed as mean ± standard deviation of three replicates. <sup>b</sup> Different lowercase letters (a-d) in the same column indicate a significant difference ( $P \leq 0.05$ ) as determined by Tukey post hoc test.



in Table 1, the surface hydrophobicity index ( $H_0$ ) increased with CP treatment duration, peaking after 6 min ( $P < 0.05$ ). The initial rise in SHI at 4 min of CP exposure can be attributed to the disintegration of reversible protein aggregates and subunits caused by plasma etching during the early treatment phase. Similar trends were observed by Ji *et al.* and Ommat Mohammadi *et al.* in their studies on peanut protein and whey protein isolate (WPI) respectively.<sup>34,35</sup> The  $H_0$  value of the untreated PPI-NP sample increased from  $1225.95 \pm 62.76$  to  $1445.85 \pm 72.39$  after 4 min of CP treatment at 30 kV. This increase is likely due to moderate oxidation during CP exposure, which induces alterations in the protein's tertiary structure and exposes hydrophobic regions previously buried within the molecule.<sup>69</sup>

However, extending CP treatment beyond 6 min led to a decline in  $H_0$  values. This decrease can be attributed to prolonged exposure and intensified oxidation, exposing additional hydrophobic regions. Consequently, insoluble protein aggregates form due to hydrophobic interactions, leading to a reduction in  $H_0$ . The decline in hydrophobicity observed after 8 min of CP treatment may be due to two factors: (1) oxidation of hydrophobic amino acid residues, producing carbonyl groups, and (2) partial refolding of protein isolates, disrupting aromatic amino acids.<sup>70</sup> Nasiru *et al.* and Cheng *et al.* documented comparable findings for egg white protein and shrimp tropomyosin following CP treatment, underscoring the consistent impact of plasma exposure on protein hydrophobicity.<sup>44,71</sup>

### 3.11. Colour

The lightness ( $L^*$ ) of PPI showed minimal changes after CP treatment, but a significant reduction in the yellow color

parameter ( $b^*$ ) was observed under all treatment conditions. Mehr and Koocheki<sup>32</sup> also reported a similar decrease in  $b^*$  after exposure to reactive species like hydroxyl radicals and ozone (Table 1). These findings align with Dong *et al.*, who found that CP treatment induced negligible color changes in PPI solutions.<sup>72</sup> However, Gong *et al.* observed an increase in the yellow hue of whey protein solutions treated with CP, which was attributed to browning effects caused by plasma-protein interactions.<sup>43</sup> The decline in  $b^*$  values of PPI-NPs after DBD plasma treatment is primarily due to the action of reactive species such as ozone ( $O_3$ ) and hydroxyl radicals (OH), along with other transient reactive intermediates. A reduction in yellowness generally improves the visual appeal of PPI-NPs, making the treated samples more aesthetically pleasing. These results align with previous research on pea protein<sup>21</sup> and WPI,<sup>54</sup> which indicated that color changes during plasma treatment are largely influenced by reaction by-products generated through plasma-protein interactions.

### 3.12. XRD analysis

XRD analysis provides valuable insights into the crystallinity of materials, making it an essential technique for evaluating the potential of a substance for biomaterial applications.<sup>1</sup> The XRD spectra of PPI-NPs before and after DBD plasma treatment are presented in Fig. 3b. XRD patterns were examined to confirm the increase in crystallinity observed in the SEM and TGA analyses. The spectra revealed the crystalline nature of the protein samples, with several prominent peaks appearing in the  $2\theta$  range of  $20^\circ$ – $30^\circ$ .<sup>73</sup> The most pronounced peak, observed at  $19.4^\circ$ , indicates the  $\beta$ -sheet structure in proteins, a finding consistent with previous studies.<sup>74</sup> Notable variations in the



Fig. 4 SEM images of (a) PPI-NPs C, (b) PPI-NPs 30 kV 4 min, (c) PPI-NPs 30 kV 6 min and (d) PPI-NPs 30 kV 8 min.



intensity of XRD peaks at 10.6°, 19.4°, and 29.2° were observed, suggesting that the increased peak intensity reflects a higher proportion of crystalline molecules in the sample.<sup>75</sup> This observation supports earlier findings that CP treatment enhances the crystallinity of the protein samples. The structural changes observed suggest that plasma treatment alters the ordered structure of the protein by disrupting specific inter- and intra-molecular bonds, thereby decreasing the regularity of the crystalline arrangement.

### 3.13. Morphological analysis of native and CP-treated PPI-NPs

SEM analysis was utilized to further investigate the microstructure of PPI-NPs. The untreated PPI-NPs displayed irregular elliptical aggregates (Fig. 4a). According to Mehr and Koocheki, CP technology effectively enhances the hydrodynamic diameter of PPI-NPs and serves as a reliable method for producing protein nanoparticles with diverse shapes and sizes<sup>32</sup> (Fig. 4b–d). As the CP treatment duration increased, the aggregates began to disperse, eventually forming an uneven flaked structure and breaking down into smaller, more irregular particles. These findings align with previous reports on pea protein isolates,<sup>11</sup> flaxseed protein,<sup>76</sup> and soy protein,<sup>67</sup> which also reported topological changes in protein aggregates following polymerization induced by CP treatment. CP treatment demonstrates significant potential in promoting protein aggregation.

## 4. Conclusions

DBD-CP technology effectively modified PPI-NPs, altering their size, morphology, and functionality. Plasma treatment introduced RONS, which facilitated forming new functional groups on the PPI-NP surface, including carboxyl and carbonyl groups. CP-treated samples exhibited higher absorbance within the 230–300 nm range, whereas the fluorescence intensity decreased with longer treatment durations. Surface hydrophobicity initially increased but diminished after prolonged treatment (8 min), while solubility improved with extended plasma exposure at 30 kV. Thermal analysis indicated that plasma exposure at 30 kV for 6 and 8 min elevated the denaturation temperature ( $T_d$ ) to 112 °C and 114 °C, respectively, compared to 110 °C in untreated samples, suggesting enhanced cross-linking of polar functional groups. Moreover, PPI-NPs treated at 30 kV for 6 min demonstrated superior absorption at the oil–water interface, resulting in a more stable interfacial layer, enhancing their emulsifying properties. However, optimizing plasma treatment conditions remains complex, as voltage, frequency, treatment duration, and distance from the plasma source significantly influence the outcomes. Additionally, scaling up plasma treatment, addressing capital costs, and ensuring the safety of plasma-exposed products are critical considerations for commercial applications.

## Data availability

Data will be made available on request.

## Author contributions

Srutee Rout: conceptualization, data curation, methodology, formal analysis, validation, writing – original draft, writing – review & editing. Prem Prakash Srivastav: supervision, visualization, writing – review & editing.

## Conflicts of interest

The authors declare that they have no known competing financial interests or personal relationships that could have appeared to influence the work reported in this paper.

## Acknowledgements

The authors would like to thank IIT Kharagpur for providing the facilities and other resources, without which it would have been difficult to complete this review article. The authors are indebted to the Ministry of Human Resource Development (MHRD), Govt. of India for an individual research fellowship (Prime Minister's Research Fellowship & Date: 18/05/22) for funding and providing the necessary facilities.

## References

- 1 A. Rasool, S. Sri, M. Zulfajri and F. S. Krismastuti, Nature inspired nanomaterials, advancements in green synthesis for biological sustainability, *Inorg. Chem. Commun.*, 2024, **112**, 954.
- 2 M. Kumar, S. Mahmood, S. Chopra and A. Bhatia, Biopolymer based nanoparticles and their therapeutic potential in wound healing—A review, *Int. J. Biol. Macromol.*, 2024, **131**, 131335.
- 3 M. Stevanović and N. Filipović, A review of recent developments in biopolymer nano-based drug delivery systems with antioxidative properties: Insights into the last five years, *Pharmaceutics*, 2024, **16**, 670.
- 4 C. Costa, N. G. Azoia, L. Coelho, R. Freixo, P. Batista and M. Pintado, Proteins derived from the dairy losses and by-products as raw materials for non-food applications, *Foods*, 2021, **10**, 135.
- 5 A. Drabczyk, S. Kudłacik-Kramarczyk, M. Jamroży and M. Krzan, Biomaterials in Drug Delivery: Advancements in Cancer and Diverse Therapies, *Int. J. Mol. Sci.*, 2024, **25**, 3126.
- 6 A. Akhtar, S. Aslam, S. Khan, D. J. McClements, N. Khalid and S. Maqsood, Utilization of diverse protein sources for the development of protein-based nanostructures as bioactive carrier systems: A review of recent research findings (2010–2021), *Crit. Rev. Food Sci. Nutr.*, 2023, **63**, 2719–2737.
- 7 S. Rout and P. P. Srivastav, Impact of cold-plasma on the nutritional, textural and structural properties of soy and pea protein isolate for the development of plant-based noodles, *J. Food Sci. Technol.*, 2025, **1**, 1.
- 8 L. Grossmann, Structural properties of pea proteins (*Pisum sativum*) for sustainable food matrices, *Crit. Rev. Food Sci. Nutr.*, 2024, **64**, 8346–8366.



- 9 S. Rout, P. K. Dash, P. K. Panda, Y. C. Yang and P. P. Srivastav, Interaction of dairy and plant proteins for improving the emulsifying and gelation properties in food matrices: a review, *Food Sci. Biotechnol.*, 2024, **33**, 3199–3212.
- 10 K. V. Bastos, A. B. de Souza, A. C. Tomé and F. D. Souza, New strategies for the extraction of antioxidants from fruits and their by-products: a systematic review, *Plants*, 2025, **14**, 755.
- 11 S. Rout and P. P. Srivastav, Modification of soy protein isolate and pea protein isolate by high voltage dielectric barrier discharge (DBD) atmospheric cold plasma: Comparative study on structural, rheological and techno-functional characteristics, *Food Chem.*, 2024, **447**, 138914.
- 12 F. Jhan, N. Jan, A. Gani, N. Noor, M. Ahmad, N. A. Bhat and B. A. Ashwar, Advances in the Application of Food Proteins and Enzymes, *Food Biopolymers: Structural, Functional and Nutraceutical Properties*, 2021, pp. 339–386.
- 13 S. Rout, P. K. Panda, P. K. Dash, P. P. Srivastav and C. T. Hsieh, Cold Plasma-Induced Modulation of Protein and Lipid Macromolecules: A Review, *Int. J. Mol. Sci.*, 2025, **26**, 1564.
- 14 F. Hashempour-Baltork, A. M. Alizadeh, M. Taghizadeh and H. Hosseini, Cold plasma technology: A cutting-edge approach for enhancing shrimp preservation, *Heliyon*, 2024, **10**, 114185.
- 15 S. Rout and P. P. Srivastav, Effect of cold plasma on the technological and functional modification of plant proteins and enzymes, *Innovative Food Sci. Emerging Technol.*, 2023, **88**, 103447.
- 16 S. Rout, S. Tripathy and P. P. Srivastav, Effect of cold plasma for modulating macromolecules and bioactive composition of food: unveiling mechanisms and synergies with other emerging techniques, *Food Biosci.*, 2024, **8**, 104545.
- 17 S. Rout and P. P. Srivastav, Cold Atmospheric Plasma Processing of Plant-Based Proteins, in *Novel Plant Protein Processing*, CRC Press, 2023, pp. 172–188.
- 18 N. Nikmaram and K. M. Keener, Aflatoxin M1 degradation using high voltage atmospheric cold plasma (HVACP) technology, *Ozone: Sci. Eng.*, 2023, **45**, 503–515.
- 19 S. Rout and P. P. Srivastav, A concise review on the thermal and non-thermal extraction methods of dietary fiber and their implications on human health, *Food Chem. Adv.*, 2023, **3**, 100466.
- 20 X. Liang, D. J. McClements, Z. Jin and L. Chen, Whey protein nanoparticles: Enhancing solubility, environmental resistance, and bio-accessibility of pterostilbene, *Food Biosci.*, 2024, **60**, 104290.
- 21 Y. Liu, J. Sun, Z. Wen, J. Wang, M. S. Roopesh, D. Pan and L. Du, Functionality enhancement of pea protein isolate through cold plasma modification for 3D printing application, *Food Res. Int.*, 2024, **197**, 115267.
- 22 C. Marques, P. Maroni, L. Maurizi, O. Jordan and G. Borchard, Understanding protein-nanoparticle interactions leading to protein corona formation: In vitro-in vivo correlation study, *Int. J. Biol. Macromol.*, 2024, **256**, 128339.
- 23 Y. R. Wu, Q. Zhou, J. Li, W. Wang, Y. B. Zhou and K. Liu, The formation of protein coronas and its effect on the quercetin-edible dock protein nanoparticles, *Food Hydrocolloids*, 2024, **157**, 110432.
- 24 Y. Y. Chen, X. Y. Li, Q. M. Li, L. H. Pan, J. P. Luo and X. Q. Zha, Dual decoration of quinoa protein isolate by different dietary polyphenols with covalent and noncovalent approaches: structure characterization, conformational changes and functional properties, *Food Hydrocolloids*, 2024, **156**, 110376.
- 25 H. R. Angourani, M. Heydari, A. R. Yousefi, B. Pashaei and A. Mastinu, Nanoparticles based-plant protein containing *Rosmarinus officinalis* essential oil; fabrication, characterization, and evaluation, *Appl. Sci.*, 2022, **12**(19), 9968.
- 26 M. M. Nasiru, E. F. Boateng, Z. Wang, W. Yan, H. Zhuang and J. Zhang, Ultrasound-assisted high-voltage cold atmospheric plasma treatment on the inactivation and structure of lysozyme: Effect of treatment voltage, *Food Bioprocess Technol.*, 2022, **15**, 1866–1880.
- 27 Y. Teng, Y. Wang, X. Xu, R. Wang, B. Chen, L. Wang, F. Zhan, Z. Han, Y. Li, X. Zhu and X. A. Zeng, Enhancement of chickpea protein functionalities through higher-intensity pulsed electric field: insights into protein aggregations and structural changes, *Food Hydrocolloids*, 2025, **111**, 111227.
- 28 L. Dong, X. Lu, A. Zeng and S. Lin, Regulation of ovalbumin allergenicity and structure-activity relationship analysis based on pulsed electric field technology, *Int. J. Biol. Macromol.*, 2024, **261**, 129695.
- 29 S. Jiang, C. Yang, R. Bai, Z. Li, L. Zhang, Y. Chen, X. Ye, S. Wang, H. Jiang and W. Ding, Modifying duck myofibrillar proteins using sodium bicarbonate under cold plasma treatment: Impact on the conformation, emulsification, and rheological properties, *Food Hydrocolloids*, 2024, **150**, 109682.
- 30 T. Lan, Y. Dong, L. Jiang, Y. Zhang and X. Sui, Analytical approaches for assessing protein structure in protein-rich food: A comprehensive review, *Food Chem.:X*, 2024, 101365.
- 31 K. K. Griendling, R. M. Touyz, J. L. Zweier, S. Dikalov, W. Chilian, Y. R. Chen, D. G. Harrison and A. Bhatnagar, Measurement of reactive oxygen species, reactive nitrogen species, and redox-dependent signaling in the cardiovascular system: a scientific statement from the American Heart Association, *Circ. Res.*, 2016, **119**, e39–e75.
- 32 H. M. Mehr and A. Koocheki, Effects of short-term and long-term cold plasma treatment on the color, structure, and Pickering foaming properties of Grass pea protein particles, *Food Hydrocolloids*, 2023, **143**, 108846.
- 33 M. Chen, J. H. Cheng and D. W. Sun, Reduced graphene oxide prepared by cold plasma green treatment in liquid phase for fluorescence biosensing of tropomyosin in shrimp, *Food Chem.*, 2025, **468**, 142458.
- 34 E. Ommat Mohammadi, S. Yeganehzad, M. A. Hesarinejad, M. Dabestani, E. Schneck and R. Miller, Effects of various types of vacuum cold plasma treatment on the chemical and functional properties of whey protein isolate with a focus on interfacial properties, *Colloids Interfaces*, 2023, **7**, 54.



- 35 H. Ji, F. Han, S. Peng, J. Yu, L. Li, Y. Liu, Y. Chen, S. Li and Y. Chen, Behavioral solubilization of peanut protein isolate by atmospheric pressure cold plasma (ACP) treatment, *Food Bioprocess Technol.*, 2019, **12**, 2018–2027.
- 36 Y. Li, B. Wang, Q. Li, X. Hu, X. Zhang and H. Pei, Insights Into Interaction of Lutein with Pea Protein Isolate in Aqueous Nanometre-Scale Dispersion: Thermal Stability, Spectroscopic, and Morphological Properties, *Food Biophys.*, 2025, **20**, 17.
- 37 S. Pasiczna-Patkowska, M. Cichy and J. Flieger, Application of Fourier Transform Infrared (FTIR) Spectroscopy in Characterization of Green Synthesized Nanoparticles, *Molecules*, 2025, **30**(3), 684.
- 38 G. Eazhumalai, R. G. Kalaivendan and U. S. Annapure, Effect of atmospheric pin-to-plate cold plasma on oat protein: Structural, chemical, and foaming characteristics, *Int. J. Biol. Macromol.*, 2023, **242**, 125103.
- 39 S. Jangra, A. Mishra, R. Mishra, S. Pandey and R. Prakash, Transformative impact of atmospheric cold plasma on mung bean seeds: Unveiling surface characteristics, physicochemical alterations, and enhanced germination potential, *AIP Adv.*, 2024, **14**(7), 5215.
- 40 M. Jahromi, M. Niakousari, M. T. Golmakani, F. Ajallouei and M. Khaledi, Effect of dielectric barrier discharge atmospheric cold plasma treatment on structural, thermal and techno-functional characteristics of sodium caseinate, *Innovative Food Sci. Emerging Technol.*, 2020, **66**, 102542.
- 41 M. M. Nasiru, E. F. Boateng, F. Alnadari, M. Umair, Z. Wang, A. M. Senan, W. Yan, H. Zhuang and J. Zhang, Dielectric barrier discharge cold atmospheric plasma treatment of egg white protein: Insights into the functional, rheological, and structural properties, *Food Bioprocess Technol.*, 2024, **17**, 955–976.
- 42 L. A. Linhares and C. H. Ramos, Unlocking insights into folding, structure, and function of proteins through circular dichroism spectroscopy—a short review, *Appl. Biosci.*, 2023, **2**, 639–655.
- 43 W. Gong, X. L. Guo, H. B. Huang, X. Li, Y. Xu and J. N. Hu, Structural characterization of modified whey protein isolates using cold plasma treatment and its applications in emulsion oleogels, *Food Chem.*, 2021, **356**, 129703.
- 44 L. Zhao, J. Zheng, W. Yan, J. Qian, J. Zhang, J. Wang, X. Sheng, V. Raghavan, X. Yang, Y. Han and T. Cao, Combined high voltage atmospheric cold plasma and ultraviolet-cold plasma inhibited *Aspergillus flavus* growth and improved physicochemical properties of protein in peanuts, *Food Chem.*, 2025, **464**, 141607.
- 45 M. Dousti, M. Bashiry, P. Zohrabi, V. Siahpoush, A. Ghaani and K. Abdolmaleki, The effect of dielectric barrier discharge (DBD) cold plasma treatment on the reduction of aflatoxin B1 and the physicochemical properties of oat, *Appl. Food Res.*, 2024, **4**, 100515.
- 46 A. K. Kuril, A. Vashi and P. K. Subbappa, A comprehensive guide for secondary structure and tertiary structure determination in peptides and proteins by circular dichroism spectrometer, *J. Pept. Sci.*, 2025, **31**, e3648.
- 47 S. Subadini, P. R. Hota, D. P. Behera and H. Sahoo, Circular dichroism spectroscopy: principle and application, in *Optical Spectroscopic and Microscopic Techniques: Analysis of Biological Molecules*, Springer Nature Singapore, 2022, pp. 19–33.
- 48 G. Eazhumalai, T. K. Ranjitha Gracy, A. Mishra and U. S. Annapure, Atmospheric pressure nonthermal pin to plate plasma system for the microbial decontamination of oat milk, *J. Food Process. Preserv.*, 2022, **46**, e16181.
- 49 W. Ji, M. Li, T. Yang, H. Li, W. Li, J. Wang and M. Ma, Effect of cold plasma on physical–biochemical properties and nutritional components of soybean sprouts, *Food Res. Int.*, 2022, **161**, 111766.
- 50 A. Hekmat, I. Kostova and A. A. Saboury, Application of metallic nanoparticles-amyloid protein supramolecular materials in tissue engineering and drug delivery: Recent progress and perspectives, *Colloids Surf., B*, 2024, **114**, 114185.
- 51 W. You, H. Liu, B. N. Kashenye, Y. Li, H. Zheng and Q. Zhang, Ultrasound-assisted preparation of zein particles: Insight into the effects and mechanisms of thermal factors, *Innovative Food Sci. Emerging Technol.*, 2024, **97**, 103825.
- 52 Y. Li, Z. He, Y. Tu, L. Chen and X. Li, Understanding synchronous regulating effects of starch-protein interactions on starch digestion and retrogradation under thermal shear processing, *Carbohydr. Polym.*, 2024, **329**, 121767.
- 53 C. Lefèvre, P. Bohuon, V. Lullien-Pellerin and C. Mestres, Modeling the thermal denaturation of the protein–water system in pulses (lentils, beans, and chickpeas), *J. Agric. Food Chem.*, 2022, **70**, 9980–9989.
- 54 S. Perinban, V. Orsat and V. Raghavan, Effect of plasma-activated water treatment on physicochemical and functional properties of whey protein isolate, *Int. J. Food Sci. Technol.*, 2023, **58**, 1346–1355.
- 55 J. Zhou, T. Yang, Z. Chen, Y. Chen and S. Li, A non-thermal modification method to promote the interaction of zein-alginate oligosaccharides composites for better encapsulation and stability—Cold plasma, *Int. J. Biol. Macromol.*, 2023, **253**, 126496.
- 56 R. Santhosh, D. M. Babu, R. Thakur, D. Nath, M. Hoque, K. K. Gaikwad, J. Ahmed and P. Sarkar, Effect of atmospheric cold plasma treatment on structural, thermal, and mechanical properties of pea protein isolate edible films, *Sustainable Chem. Pharm.*, 2024, **37**, 101398.
- 57 N. F. Zainal, J. M. Saiter, S. I. Halim, R. Lucas and C. H. Chan, Thermal analysis: basic concept of differential scanning calorimetry and thermogravimetry for beginners, *Chem. Teach. Int.*, 2021, **3**, 59–75.
- 58 Y. Chen, X. L. Cai, L. Liu, T. Zhang, L. K. Qin and Y. L. Jia, Preparation and performance characterization of insoluble dietary fiber–alginate–pea protein ternary composite gels, *Food Hydrocolloids*, 2025, **160**, 110852.
- 59 S. Boostani, K. Sarabandi, O. Tarhan, A. Rezaei, E. Assadpour, H. Rostamabadi, S. R. Falsafi, C. Tan, F. Zhang and S. M. Jafari, Multiple Pickering emulsions



- stabilized by food-grade particles as innovative delivery systems for bioactive compounds, *Adv. Colloid Interface Sci.*, 2024, 103174.
- 60 J. J. Yu, P. Y. Jiang, S. H. Li and Y. Chen, Mechanism of improving interfacial hydration characteristic of high-denatured peanut protein induced by cold plasma, *J. Food Process Eng.*, 2022, 45, e13926.
- 61 P. Kumar, P. Srikar, D. Dahatonde, R. K. Gangwar and T. Nallamilli, Effect of atmospheric pressure cold plasma treatment on charge, structure, thermal properties and coacervation behavior of Pea protein isolate with Alginate, *Innovative Food Sci. Emerging Technol.*, 2025, 103948.
- 62 P. Rachtanapun, C. Rachtanapun, P. Jantrawut, S. Thanakkasaranee, G. Kasi, J. Tantala, P. Panraksa and T. Chaiwarit, Carboxymethyl chitosan-based materials in packaging, food, pharmaceutical, and cosmetics, in *Multifaceted Carboxymethyl Chitosan Derivatives: Properties and Biomedical Applications*, Springer Nature Switzerland, 2023, pp. 139–203.
- 63 W. Wang, R. Sun, S. Ji and Q. Xia, Effects of  $\kappa$ -carrageenan on the emulsifying ability and encapsulation properties of pea protein isolate-grape seed oil emulsions, *Food Chem.*, 2024, 435, 137561.
- 64 J. Li, Z. Wang, N. Xiao, S. Guo and M. Ai, Endogenous reactive oxygen species (ROS)-driven protein oxidation regulates emulsifying and foaming properties of liquid egg white, *Int. J. Biol. Macromol.*, 2024, 268, 131843.
- 65 C. A. He, J. R. Qi, J. S. Liao, Y. T. Song and C. L. Wu, Excellent hydration properties and oil holding capacity of citrus fiber: Effects of component variation and microstructure, *Food Hydrocolloids*, 2023, 144, 108988.
- 66 J. J. Yu, H. Ji, Y. Chen, Y. F. Zhang, X. C. Zheng, S. H. Li and Y. Chen, Analysis of the glycosylation products of peanut protein and lactose by cold plasma treatment: Solubility and structural characteristics, *Int. J. Biol. Macromol.*, 2020, 158, 1194–1203.
- 67 Q. Zhang, Z. Cheng, J. Zhang, M. M. Nasiru, Y. Wang and L. Fu, Atmospheric cold plasma treatment of soybean protein isolate: Insights into the structural, physicochemical, and allergenic characteristics, *J. Food Sci.*, 2021, 86, 68–77.
- 68 X. Y. Liu, T. S. He, C. C. Wang, B. C. Xu, R. Feng, B. Zhang and H. Tao, Modulation of pea protein isolate nanoparticles by interaction with OSA-corn starch: Enhancing the stability of the constructed Pickering emulsions, *Food Chem.*, 2024, 437, 137766.
- 69 H. Zhang, X. Zhao, X. Chen and X. Xu, Thoroughly review the recent progresses in improving O/W interfacial properties of proteins through various strategies, *Front. Nutr.*, 2022, 9, 1043809.
- 70 Y. Wang, N. Wang, B. Liu, C. Han, T. Wang, M. Pan and D. Yu, Effect of ohmic heating-assisted glycation reaction on the properties of soybean protein isolate-chitosan complexes, *Int. J. Biol. Macromol.*, 2024, 283, 137859.
- 71 J. H. Cheng, J. Li and D. W. Sun, Effects of dielectric barrier discharge cold plasma on structure, surface hydrophobicity and allergenic properties of shrimp tropomyosin, *Food Chem.*, 2023, 409, 135316.
- 72 S. Dong, A. Gao, Y. Zhao, Y. T. Li and Y. Chen, Characterization of physicochemical and structural properties of atmospheric cold plasma (ACP) modified zein, *Food Bioprod. Process.*, 2017, 106, 65–74.
- 73 G. Shan, Z. Xu, L. Jiang, Y. Zhang and X. Sui, Fabrication and characterization of glycerin-plasticized soy protein amyloid fibril scaffolds by unidirectional freeze casting method, *Food Hydrocolloids*, 2024, 147, 109400.
- 74 G. Karabulut, Advancing sustainable packaging through self-assembly induced amyloid fibrillization of soy and pea protein nanofilms, *Food Chem.*, 2025, 463, 141302.
- 75 Z. Tang, D. Yang, W. Tang, C. Ma and Y. C. He, Combined sulfuric acid and choline chloride/glycerol pretreatment for efficiently enhancing enzymatic saccharification of reed stalk, *Bioresour. Technol.*, 2023, 387, 129554.
- 76 X. Yu, S. Huang, C. Nie, Q. Deng, Y. Zhai and R. Shen, Effects of atmospheric pressure plasma jet on the physicochemical, functional, and antioxidant properties of flaxseed protein, *J. Food Sci.*, 2020, 85, 2010–2019.

